PHYSICAL REVIEW A VOLUME 40, NUMBER 1 JULY 1, 1989

Chaos and chaotic transients in an yttrium iron garnet sphere

T. L. Carroll, L. M. Pecora, and F. J. Rachford
Materials Physics Branch, U.S. Naval Research Laboratory, Washington, D.C. 20375
(Received 28 November 1988)

We present detailed results of studies of chaos and chaotic transients involving spin waves in an yttrium iron garnet sphere. We drive the ferromagnetic resonance of this system at the first-order Suhl instability using driving frequencies between 2.0 and 3.4 GHz. In some regions of parameter space we see chaotic transients, while in others we see quasiperiodic oscillations or stable chaos. We characterize these states by various means, such as dimension or amplitude. We also present some results of a three-spin-wave-mode calculation based on the Landau-Lifshitz equation. This calculation produces phenomena similar to some of those seen in the experiment but is not sufficient to reproduce all the behavior that we see. We believe that a calculation involving more spin-wave modes is necessary to reproduce many of our experimental results.

INTRODUCTION

It has been known since the 1950s that spheres of yttrium iron garnet (YIG), when used in ferromagnetic resonance experiments, display a breakdown of the ferromagnetic resonance line at high radio-frequency (rf) powers and exhibit unusual behavior, such as auto-oscillations, above the breakdown power.[1,2] The onset of this breakdown was explained by Suhl,[3] but the nature of the auto-oscillations (which, despite their name, may not be periodic), as well as much other complex behavior, was not understood at the time. More recently, Gibson and Jeffries[4] demonstrated that some of this unexplained behavior could also be seen in nonlinear flows and maps. Other experiments[5-10] have expanded the range of phenomena in YIG spheres that can be modeled using techniques from nonlinear dynamics.[11-14] The use of the methods of nonlinear dynamics to explain problems in solid-state physics has been reviewed by Jeffries[15] and Zettl.[16]

We have investigated the behavior of pure single-crystal spheres of YIG in parameter regions not covered by any previous experiments, and have seen phenomena not seen in these other studies. Research that we have published so far centers on transient chaos,[5-7] produced when initial conditions place the system on an unstable chaotic attractor that overlaps the basins of attraction of one or more stable nonchaotic attractors. In certain parameter regimes, this unstable chaotic attractor can dominate the behavior of the system for very long times, even though asymptotically, only nonchaotic attractors determine the stable phase-space trajectories. In this paper we describe in more detail how the unstable chaotic attractor influences the spin-wave properties of the YIG spheres, as well as how the system behaves when the unstable chaotic attractor is not present.

When a sample of yttrium iron garnet, a ferrimagnetic material, is placed in a dc magnetic field, the magnetic moment of the YIG will precess uniformly about the dc field. Because of damping, this motion will die out unless a rf magnetic field is applied (perpendicular to the dc field in our experiment). For a dc field on the order of 1000 G, the resonance frequency is between 2 and 4 GHz when the easy axis (the [111] axis) of magnetization of the YIG sphere is parallel to the dc field. In our experiment, we keep the rf field tuned to the resonant frequency as we change the dc magnetic field.

Motion of a magnetic moment in a magnetic field may be described by the Landau-Lifshitz equation:[1,2]

$$\frac{d\mathbf{m}}{dt} = -\gamma \mathbf{m}\times\mathbf{H}_{\text{eff}} - \alpha\mathbf{m}\times(\mathbf{m}\times\mathbf{H}_{\text{eff}}) , \tag{1}$$

where γ is the gyromagnetic ratio and α is a damping parameter. In this case, H_{eff} includes the applied dc field, the applied rf field, the exchange field, and the dipole field. Because the [111] axis of the crystal sphere is parallel to the applied dc field, the anisotropy field is combined with the term for the dc field when the magnitude of the dc field is well above the saturation magnetization of the sphere. A situation when the dc field is not well above this value is mentioned below.

For small rf fields, only uniform precession is present. The Suhl instability,[3] responsible for the breakdown of the ferromagnetic resonance line, occurs at a higher rf power. At this power the nonlinearity in the Landau-Lifshitz equation couples the uniform mode of precession into spin-wave modes, which are spatially periodic variations in the amplitude or phase of the precession. At the first-order Suhl instability, the rate of transfer of energy from the uniform mode into the spin-wave modes goes as first order in the amplitude of the uniform mode and the first spin waves to be excited have a frequency half that of the driving frequency. From the linear part of the Landau-Lifshitz equation one may obtain a dispersion relation for the spin waves:

$$\omega_k = \left[\left[\omega_0 - \frac{\omega_m}{3} + \gamma\beta k^2 \right] \times \left[\omega_0 - \frac{\omega_m}{3} + \beta\gamma k^2 + 2\omega_m \sin\theta_k \right] \right]^{1/2} ,$$

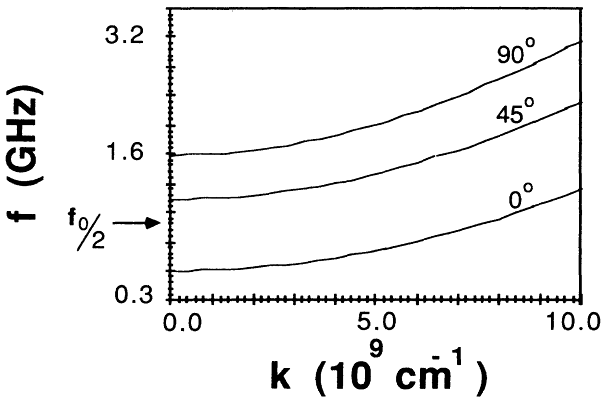

FIG. 1. Spin-wave dispersion relation for three different values of θ_k. Arrow shows where first spin waves are excited when the system is driven at 2.0 GHz.

where $\omega_0=\gamma H_{dc}$, k and ω_k are the wave number and frequency of some spin-wave mode, $\omega_m=4\pi\gamma M_s$, $\beta=H_{ex}a^2/M_s$, a is the lattice parameter, M_s is the saturation magnetization, γ is the gyromagnetic ratio, and θ_k is the angle between the spin-wave vector k and the dc field. As θ_k is varied from 0° to 90°, the dispersion relation sweeps the spin-wave manifold. We have chosen our rf frequencies so that for a wave vector $k\approx 0$, the first spin waves to be excited lie within this spin-wave manifold, as pictured in Fig. 1. This makes it possibles to excite spin waves of relatively low wave vector, so that the Suhl instability occurs at small rf magnetic fields on the order of tens of mOe.[2] When two or more of these spin-wave modes are excited, their interaction produces a high-frequency (GHz) signal modulated by a lower-frequency (kHz) signal, which, although it may not be periodic, is known as an auto-oscillation. These auto-oscillations, with frequencies ranging from 5 to 300 kHz, are what we detect.

EXPERIMENTAL PROCEDURE

In this experiment, a 20-mil-diam undoped single-crystal YIG sphere was held with Apiezon M grease inside a quartz tube so that the YIG sphere was between an excitation coil and an orthogonal pickup coil. These coils formed provided a nonresonant means to drive the precession of the magnetic moment. An electromagnet provided a dc field perpendicular to both coils and parallel to the easy axis of the YIG sphere. Microwave power was provided by a HP 8341A synthesized sweeper. The signal induced in the pickup coil by the YIG sphere was detected by a crystal detector and amplified. The signal was digitized at 3 MHz with a Lecroy TR8828C digitizer with 8 bit resolution to produce a time series of up to 131 072 points that was transferred to a VAX 11/780 computer. Figure 2 is a schematic of the experimental setup. All measurements were made with the system tuned to the center of the ferromagnetic resonance line located in the range 2.0–3.3 GHz. The YIG sphere was undercoupled to the pickup and excitation coils (the coupling constant between the sphere and the excitation coil was 0.4; for the pickup coil it was 0.01). We saw the same behavior when the excitation coil coupling was reduced to one tenth the above value, suggesting that coupling between the sphere and the excitation coil is not important for the phenomena that we see. To ensure reproducibility, two different 20-mil spherical samples were used.

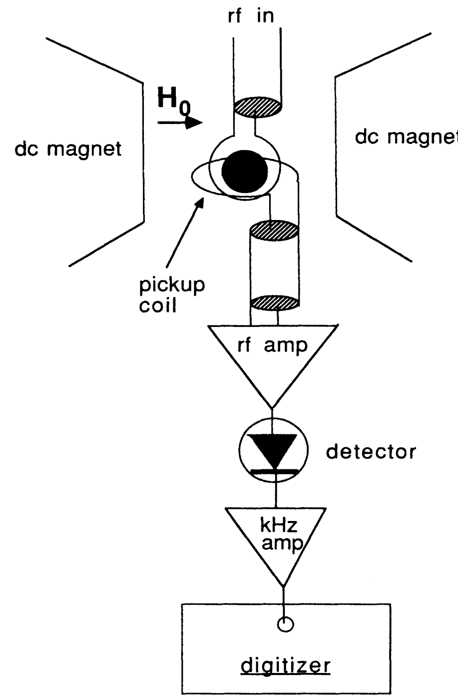

FIG. 2. Schematic of the experiment. YIG sphere is represented by the black disk in between the magnet poles.

METHODS OF ANALYSIS

Our analysis of this system depends on several ideas from the field of nonlinear dynamics. The most important of these is that over time the behavior of a dissipative dynamical system will occupy a bounded region in phase space known as an attractor.[17] If all variables of the motion are known, this attractor may be constructed by plotting the value of each variable on an orthogonal axis and following these variables for some time. If a time series in only one variable exists (for example, V_1, V_2, $V_3,\ldots$), a topologically equivalent attractor may be constructed in a D-dimensional phase space by choosing a delay of n data points and plotting the end points of the D-dimensional vector[18] $(V_i, V_{i+n}, V_{i+2n},\ldots, V_{i+(D-1)n})$. In many cases, studying these attractors is more useful than observing many of the usual quantities used in signal analysis, such as Fourier transforms. Figure 3(a) shows a reconstruction in a three-dimensional embedding space of a typical quasiperiodic auto-oscillation for this system. Figure 3(b) is a reconstruction of a chaotic attractor. Figure 3(c) is a reconstruction of

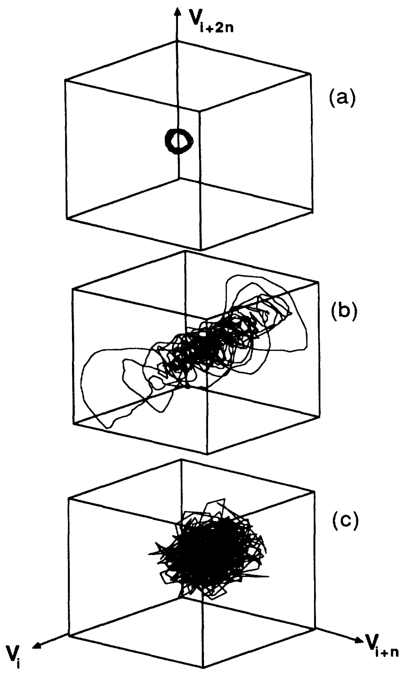

FIG. 3. (a) Three-dimensional phase-space reconstruction of a quasiperiodic attractor with a dimension of 4. (b) Reconstruction of a chaotic attractor with a dimension of 3.3. (c) Reconstruction of amplifier noise.

digitized amplifier noise, shown for comparison with the chaotic attractor. These attractors are all plotted with the same delay of $n = 8$ data points. The individual data points were taken every 320 ns.

Analysis of these reconstructed attractors is a field that is still under development. Many techniques require excessive computer time or higher resolution data than we have been able to acquire. The most useful method that we have found so far is the calculation of information dimension.[19] We have used the method of Termonia and Alexandrowicz,[20] in which one chooses many random centers on the attractor and determines the distance to the nearest neighbor, the next nearest neighbor, etc. for all data points. Averaging neighbor distances for all centers, one then plots the log of neighbor order versus the log of the distance for different embedding dimensions. The slope of this curve is the information dimension of the attractor. If the dimension of the embedding space is too low, the slope of this curve increases as the dimension of the embedding space increases. The slope will saturate when the dimension of the embedding space is large enough to completely describe motion on the embedded attractor.

Figure 4 is an example of this calculation for a chaotic attractor from experimental data with a dimension of approximately 3.3. For periodic or quasiperiodic time series, the dimension calculated this way corresponds to the number of fundamental frequencies present in the waveform. In a chaotic time series, the minimum embedding dimension reveals the number of degrees of freedom necessary to produce that chaotic motion. The low resolution of our data makes it hard to determine exactly at which embedding dimension the attractor dimension saturates. Our best estimate of the minimum embedding dimension necessary to represent the chaotic motion is 8.

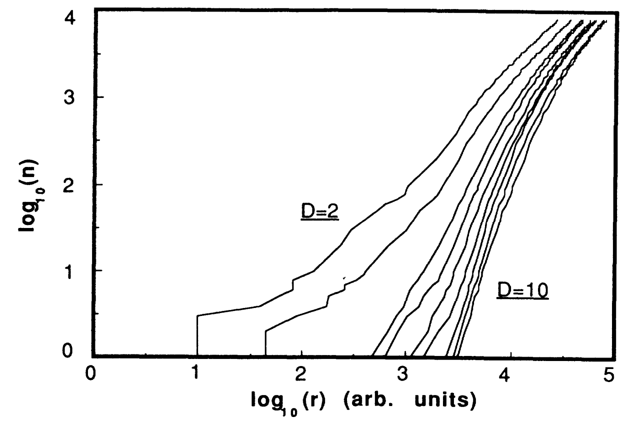

FIG. 4. Plot of the log (base 10) of the order of a neighboring phase-space point (n) vs the log of the distance to that neighbor (r) for a chaotic attractor. The slope of this plot is the dimension of the attractor.

MAP OF PARAMETER SPACE

In order to observe how different external parameters affect the nonlinear behavior of yttrium iron garnet, this behavior was mapped out by varying driving frequency and rf power, all while changing the applied dc magnetic field to keep the system tuned to the ferromagnetic resonance. The resulting map of the parameter space in Fig. 5 shows three major regions. In the nontransient region (labeled "auto-oscillations" in Fig. 3) only quasiperiodic

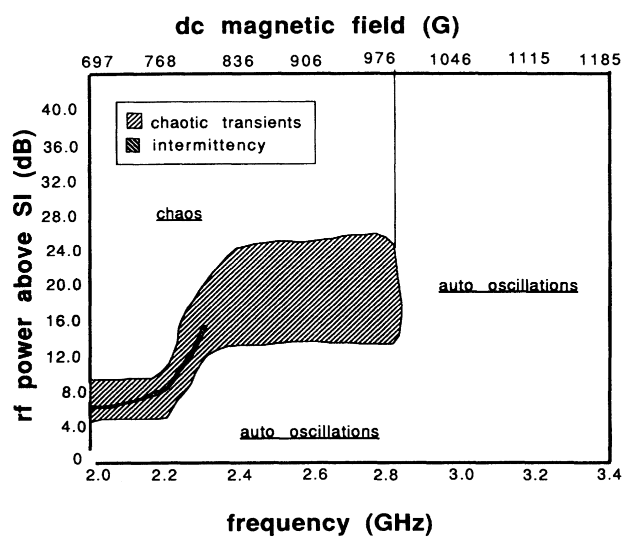

FIG. 5. Parameter space map for the ferromagnetic resonance in a yttrium iron garnet sphere. Microwave driving frequency and dc magnetic field vary simultaneously to keep the system tuned to the center of the ferromagnetic resonance line.

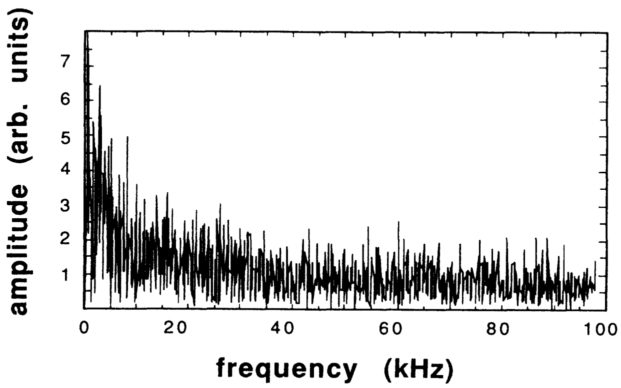

FIG. 6. Fourier amplitude spectrum for chaos.

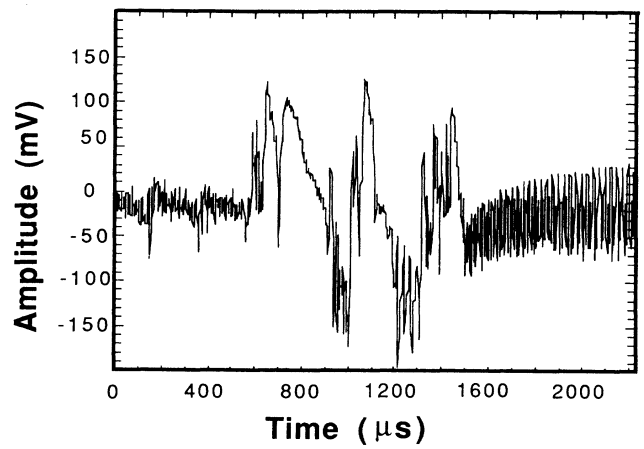

FIG. 7. Chaotic transient observed while steadily increasing rf driving power.

auto-oscillations were seen. This bottom of this region is only approximate. At any specific rf frequency, the exact power for the onset of auto-oscillations varied greatly with only small variations of the dc magnetic field. In the transient region (shaded in Fig. 3) chaotic transients were seen. There is also a region where only chaotic waveforms were seen (labeled "chaos" in Fig. 3). Figure 6 shows a typical Fourier spectrum of chaos seen in this experiment.

Chaos and auto-oscillations have been seen in other spin-wave experiments.[4-10] A striking feature of this parameter space map is the presence of chaotic transients, in which the system behaves chaotically for some time and then suddenly switches permanently into a quasiperiodic oscillation. This behavior has not been seen in previous spin-wave experiments (which investigated other regions of parameter space) and has been reported in only a few other experiments,[21] although some theories predict that they could be a feature of many nonlinear systems.[22-24]

Finally, it should be noted that when the rf driving frequency was between 2.8 and 3.4 GHz, no chaos was seen at the rf driving powers available to us for this experiment.

CHAOTIC TRANSIENTS

Chaotic transients were seen in the transient region during transitions between different quasiperiodic auto-oscillations that were induced by steadily increasing rf driving power[6] (Fig. 7). As rf power was steadily increased, a quasiperiodic auto-oscillation would suddenly change into chaos. This chaos would persist for some time until it would suddenly change into another quasiperiodic auto-oscillation. In Fig. 7, rf power is increasing with time, but the chaotic transient would still end in a quasiperiodic oscillation if the increase in rf power was stopped after the start of the transient. In fact, we could also observe chaotic transients by turning on the rf power suddenly[5] to a fixed power level. The particular auto-oscillation seen after a chaotic transient was not related to the auto-oscillation present before the transient, nor did the sequence of events seen when increasing rf power reverse itself when decreasing rf power.

These transients could not be initiated by perturbing the system with white noise or magnetic pulses as large as 0.3 G, leading us to conclude that these transients were not random or noise-induced events, but were a product of the internal dynamics of the system. The lengths of all chaotic transients fit the distribution $\mathcal{P}(t) \sim \exp(-t/\langle t \rangle)$ for fixed driving and dc fields.

After the end of a chaotic transient, many different auto-oscillations could be seen, but all fit into one of two types. Type-A auto-oscillations had an amplitude approximately four times as large as type-B auto-oscillations. The attractors corresponding to type-A auto-oscillations had a dimension of 4, while the attractors corresponding to type-B auto-oscillations had a dimension of 5. The measured dimensions were not exactly integers, but because the Fourier spectra of these auto-oscillations consisted of discreet lines, these numbers were rounded off to the nearest integer.

According to the theories of Grebogi, Ott, and Yorke,[22-24] a chaotic transient results when a stable chaotic attractor is made unstable by overlapping the boundary of the basin of attraction of another, stable, attractor. When the initial conditions place the system on the unstable chaotic attractor, the system will follow the chaotic trajectory until it reaches the boundary of the basin of attraction of the stable attractor. At his time, the system begins to follow a path on the stable attractor, and the chaotic transient ends. For our system, the final stable attractor corresponds to a quasiperiodic auto-oscillation. The exact length of the chaotic transient depends on the initial conditions. As rf driving power increases, the overlap between the chaotic attractor and the basin of attraction of the nonchaotic attractor decreases, until at some critical power P_c, the overlap is zero and the chaotic attractor is stable. This scenario constitutes a route to chaos via a crisis.

In this model, the average length of the chaotic transients should increase as rf driving power increases according to the power law $\langle t \rangle = K/(P_c - P)^{\gamma}$, where P_c is the critical power, P is the rf driving power, and γ is the critical exponent. In our experiment,[5–7] two classes of quasiperiodic attractors are seen after the end of the chaotic transient, a situation which the above power law can be extended to fit. In Fig. 8(a) the average transient lengths from our experiment versus. rf driving power are fit to the two-attractor power law

$$\langle t \rangle = \frac{K_1 K_2}{K_2(P_{c1}-P)^{\gamma_1}+K_1(P_{c2}-P)^{\gamma_2}} ,$$

where (in decibel units) $P_{c1}=21.8$ dB above the Suhl instability, $P_{c2}=25.9$ dB above the Suhl instability, $\gamma_1=13.0$, and $\gamma_2=6.1$. P_{c1} and γ_1 are the critical power and critical exponent for the chaotic transient to fall into a type-A attractor, while P_{c2} and γ_2 are the critical power and exponent for the chaotic transient to fall into a type-B attractor. The power-law parameters were independent of both the driving frequency between 2.3 and 2.8 GHz and the method by which the transients were excited.

Below a driving frequency of 2.3 GHz, the transient length versus driving power curve no longer fit this type of power law (Fig. 9). The rf power at which the average transient length was 5 ms decreased from 14 dB above the Suhl instability at frequencies above 2.3 GHz to 4 dB above the Suhl instability at frequencies below 2.3 GHz, while the onset of stable chaos decreased from 26 to 9 dB. Intermittency was also observed over a very narrow power region between 2.0 and 2.3 GHz.

These changes in the behavior of chaotic transients at lower frequencies are roughly correlated with an increase in the width of the ferromagnetic resonance line at a driving power below the Suhl instability. Figure 10 shows the full width at half maximum of this line as a function of rf frequency. This width drops as the driving frequency increases, leveling out at 1.2 G near 2.3 GHz. This increase in line width at lower frequencies is probably related to the very small internal magnetic field in the YIG sphere below 2.3 GHz. The internal dc magnetic field in a ferromagnetic sphere[1] is $H_0-(4\pi/3)M_s$, where H_0 is the applied dc field and $4\pi M_s$, the saturation magnetization, is 1780 G in our sphere. This internal field therefore goes to zero at an applied dc field of 593 G (a resonant frequency near 1.7 GHz) and the small anisotropy fields due to crystalline imperfections, etc., cause the magnetization to break up into domains. These extra anisotropy fields may also be felt when the internal magnetization is small, leading to a broadening of the ferromagnetic reso-

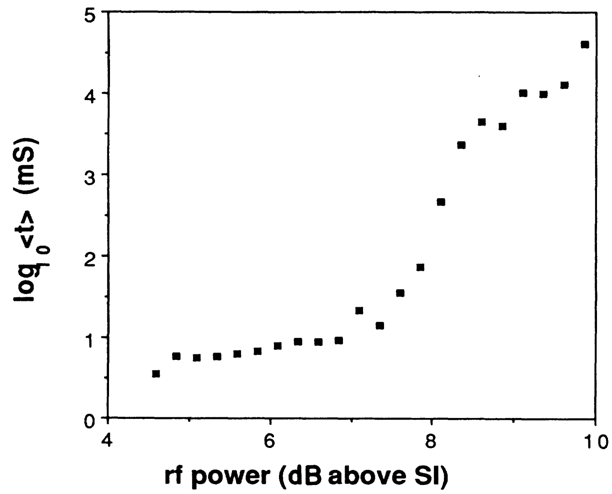

FIG. 9. Average length of chaotic transients at 2.2 GHz. Each point represents an average over 40 transients.

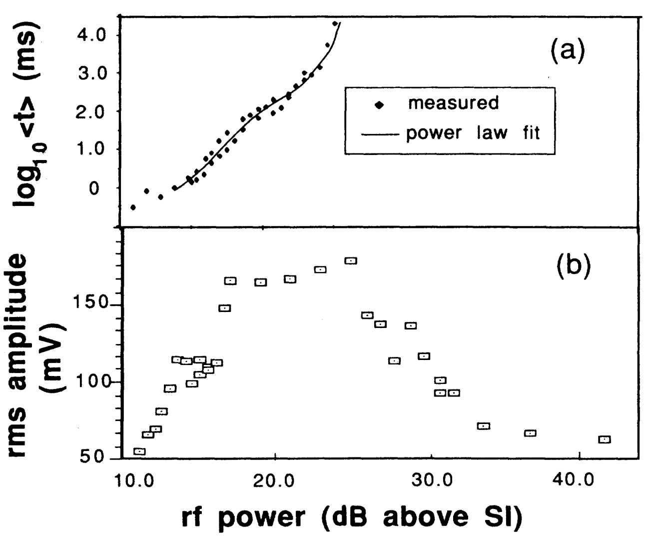

FIG. 8. (a) Average length of chaotic transients at 2.5 GHz. Each point represents an average over 40 transients. Line represents a fit to a two-attractor power law. (b) rms amplitude of the chaotic time series as rf power increases.

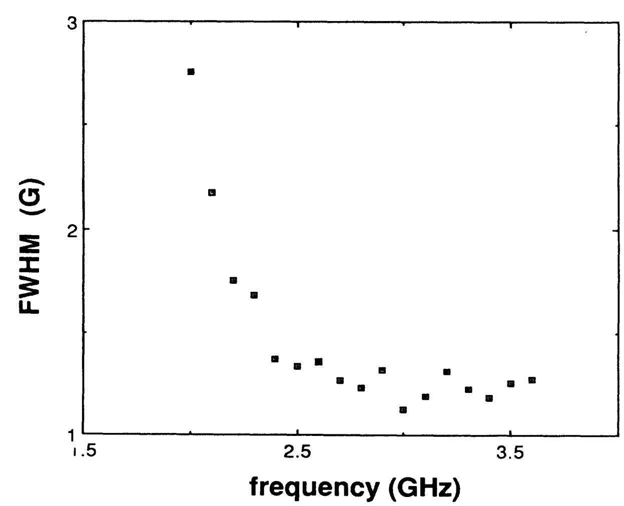

FIG. 10. Full width at half maximum of the ferromagnetic resonance line in YIG at different frequencies. All widths are taken at least 3 dB below the Suhl instability.

nance line. These anisotropy fields should complicate the spin-wave behavior, and might be responsible for some of the changes in behavior that we see below 2.3 GHz.

NONTRANSIENT BEHAVIOR

We did not see any chaos or chaotic transients in this system between 2.8 and 3.4 GHz. If the spin-wave system can become chaotic in this frequency range, it will only do so for microwave driving powers greater than those available to us (200 mW at the output of our source, or about 20 mW at the sample). Because there is no unstable chaotic attractor that the system can fall into when one quasiperiodic attractor becomes unstable, the route by which transitions between different auto-oscillations are made as driving power increases is different in the nontransient region than it was in the transient region.

Figure 11 shows Fourier transforms of a transition in the nontransient region.[6,7] Figure 11(a) is a Fourier transform of the original stable auto-oscillation. In Fig. 11(b) one can see the Fourier components of the original auto-oscillation, along with an increased background noise level and Fourier components from a new auto-oscillation. As rf power continues to increase, the noise and Fourier components of the original auto-oscillation shrink in amplitude, leaving a new stable auto-oscillation, whose Fourier transform is seen in Fig. 11(c). Some hysterisis is present during this transition. This transition is not transient; if the rf power stops increasing while the system is in the state seen in Fig. 11(b), the system will stay in this state. The lack of intermodulation between the two auto-oscillations suggests that the spin-wave system is moving back and forth between two independent attractors. Effects such as the increased background noise level during this process have been attributed in other systems to fractal basin boundaries between the two attractors.

As the rf driving power increases, the amount of noise present during these transitions increases. Beyond about 30 dB above the Suhl instability, these noisy transitions occur so close together that only a very noisy state is seen. We do not see any unique sequence of attractors as rf power is increased, but this may be due to the great sensitivity of this system to the external parameters. A dc magnetic field change as small as 0.05 G may change the auto-oscillation present.

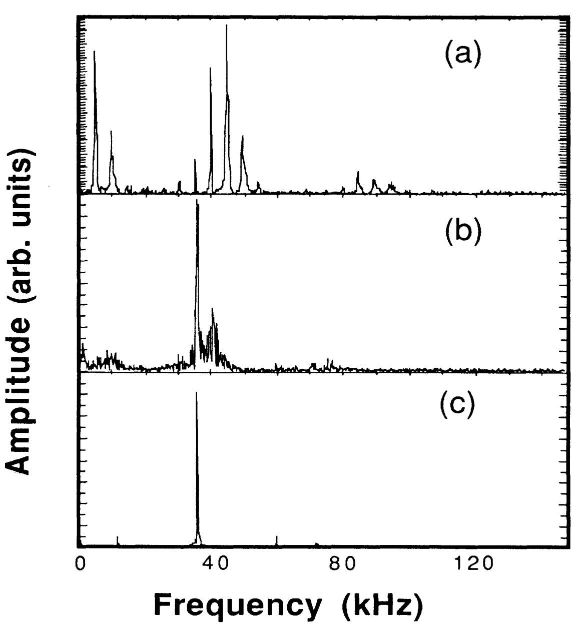

FIG. 11. Series of Fourier amplitude spectra for a nontransient transition between two auto-oscillations as driving power steadily increases. (a) Spectrum for the original auto-oscillation. (b) Spectrum of a noisy state during the transition. (c) Spectrum of the final auto-oscillation seen after the transition.

MICROWAVE REFLECTION COEFFICIENT

The presence or absence of an unstable chaotic attractor affects other aspects of the behavior of this system as well. Associated with the transitions that occur via chaotic transients are sudden changes in the microwave signal reflected from the sample. Figure 12 shows the reflection coefficient of the YIG sample as a function of rf power as power is swept up above the Suhl instability. The sudden jumps and dips in the reflection coefficient occur when the spin-wave system changes from one auto-oscillation to another via a chaotic transient.[25] These sudden changes are seen only in the transient region; in the parameter region where chaotic transients are not present, the reflection coefficient is a smooth function of power.

As with the transitions between auto-oscillations, the locations of these sudden changes are not the same for every power sweep. If 40 power sweeps (taken at 200 ms to sweep through 20 dB) are averaged together, however, some sharp features remain in the time-averaged

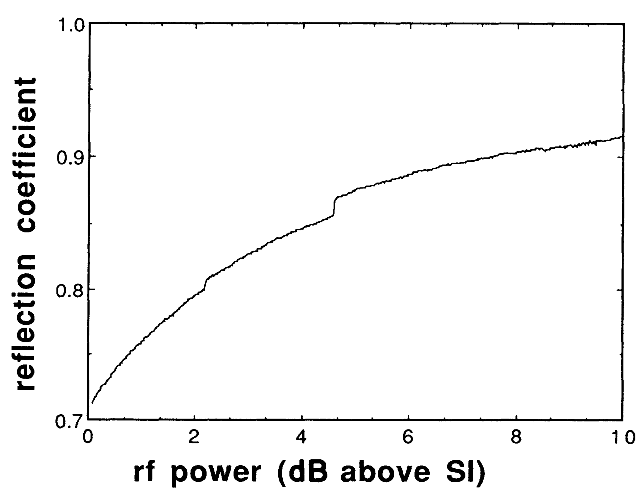

FIG. 12. Reflection coefficient of an YIG sphere at 2.5 GHz as rf power is steadily increased, showing sudden changes. This is a single power sweep, not the time-averaged result.

reflection coefficient, indicating that on this time scale, some of the chaotic transitions vary about some average location.

The first sudden change in reflection coefficient comes at about 6 dB above the Suhl instability. Even in the time-averaged reflection coefficients, there is a great deal of variation in the location of the first sharp change, but this number does seem to be a good lower limit on the power at which the first change is seen. These variations obscure any change in this location that might be present at different rf frequencies.

CHAOTIC ATTRACTOR

Some properties of the chaotic attractor itself change as rf driving power increases. We use the term "chaotic attractor" to refer both to the stable chaotic attractor present at high rf driving powers and the unstable chaotic attractor present during chaotic transients. Figure 8(b) shows the rms amplitude of the chaotic waveforms that we observed as a function of rf driving power at a driving frequency at 2.5 GHz.

Up to a certain power, the amplitude of the chaotic waveform increases with power. The breaks in this rising curve occur at approximately the same locations as the critical powers found in the power-law fit to the average transient length as a function of power [Fig. 8(a)]. In the same rf power range that Fig. 8(a) shows the overlap between the unstable chaotic attractor and the basin of attraction of the class-A attractor decreasing, Fig. 8(b) shows the amplitude of the chaotic waveform increasing. At the power above which the chaotic attractor no longer overlaps the basin of attraction of the class-A attractor, both curves have a smaller positive slope than they did below this power. Above the rf power at which the chaotic attractor no longer overlaps the basin of attraction of any other attractor, its amplitude is seen to decrease. The lowest break in the amplitude versus power curve (near 11 dB) may be caused by the presence of a third class of nonchaotic attractor whose basin of attraction also overlaps the chaotic attractor. There is a similar break in the transient length versus power curve at about the same location.

The chaos size versus power curve does not fit a power-law curve as the transient length versus power curve does. Attempts to subtract out a decreasing background curve based on the decreasing amplitude of the chaos at high power were not successful at converting the low power curve into a power-law form. Nevertheless, the data in Figs. 8(a) and 8(b) do suggest a relation between the amplitude of the chaotic time series and the degree to which it overlaps the basins of attraction of nonchaotic attractors.

Figure 13 shows the dimension of the chaotic waveforms as a function of power. This calculation required too much data to be used with the shortest chaotic transients. The dimension of the chaos is 3.3 ± 0.2 up to about 35 dB above the Suhl instability, at which point the dimension begins to increase. The minimum embedding dimension required to measure the attractor's dimension is 8. An embedding dimension of 8 implies that 8 degrees of freedom are present, so that this chaos is the product of an interaction between at least four spin-wave modes, each with a real and imaginary part.

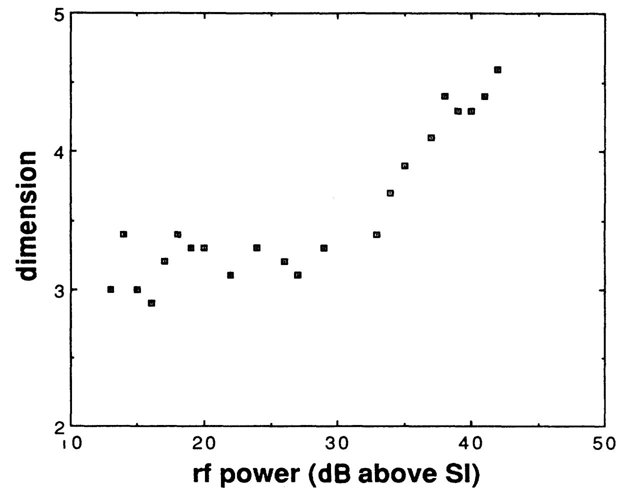

FIG. 13. Dimension of chaos and chaotic transients at 2.5 GHz as a function of driving power.

FREQUENCY-DEPENDENT EFFECTS

Unless otherwise noted, the properties of the chaotic attractor described previously vary little between driving frequencies of 2.3 and 2.8 GHz. Different behavior is seen between 2.0 and 2.3 GHz. The effects seen at 2.2 GHz are typical of, although not identical to, the type of behavior seen in this lower-frequency region.

Figure 14 shows the rms amplitude of chaos versus power at 2.2 GHz. The rms amplitude of the chaotic waveform at 2.2 GHz varies little until about 28 dB above the Suhl instability, at which point the amplitude of the chaotic waveform increases discontinuously. Above the power at which this sudden increase occurs, the amplitude of the chaotic signal decreases rapidly but

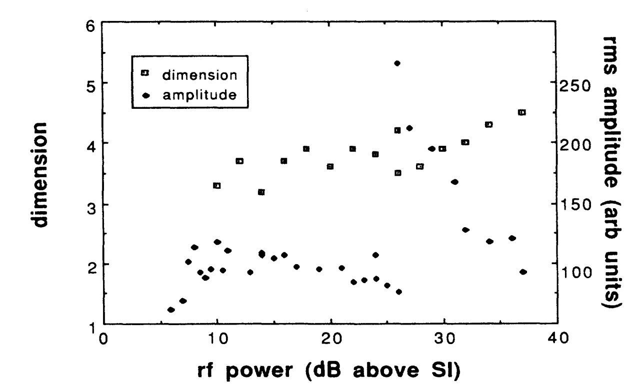

FIG. 14. Dimension and rms amplitude of chaos in an YIG sphere at 2.2 GHz.

continuously. Figure 14 also shows the dimension of the chaos as a function of power, showing the same tendency to increase at higher power as the dimension of chaos at 2.5 GHz. Figure 9 contains the average length of chaotic transients as a function of driving power at 2.2 GHz. This plot cannot be fit by a combination of power-law curves as the equivalent plot for chaotic transients at 2.5 GHz. Comparing Fig. 9 and 14 to Fig. 8 reveals large differences between the behavior of this system at driving frequencies below 2.3 and above 2.3 GHz. It was proposed above that some of these differences might be caused by the large effects of anisotropy fields being felt when the dc magnetic field dropped below a certain value.

THREE-MODE SPIN-WAVE MODEL

Our experimental situation is one of an undercoupled YIG sample, driven at resonance through the first-order Suhl instability. The equations of motion for spin-wave modes available in the literature do not cover this specific situation, necessitating a new derivation (e.g., the uniform mode will now couple to other modes, leading to different terms in the equations than in the nonresonance situation). This derivation is complicated and lengthy, so in this paper we have included only a study of a simple set of equations of motion, the "three-mode" case. This was developed using a spin-wave expansion for the magnetization following Suhl.[3]

It turns out that the three-mode model is not sufficient to see most of the rich behavior in the experiment, but does model well some of the lower power behavior and appears to exhibit the same transition to chaos (via crisis) as the experiment.

The development of the equations of motion[26] is well covered in Ref. 3 as well as by Bryant *et al.*[8], Zhang and Suhl,[13,14] and Pecora[27] so we give only an outline here. The damping term is added at the end of the derivation in the usual way.[13,14]

The first step is to rewrite the equations using the normalized magnetization $\mathbf{m}$ $(=\mathbf{M}/|\mathbf{M}|)$ and to change variables. The new variables come from the projection of the magnetization onto the x-y plane in complex coordinates: $m_+=m_x+im_y$ and $m_-=m_x-im_y$. We use the relationship $m_z=(1-m_+m_-)^{1/2}$ to generate the expansion approximation of $m_z\sim 1-m_+m_-/2$ to eliminate m_z from the equations. This is possible since $|\mathbf{M}|$ is conserved.

The second step is to substitute a spin-wave expansion of m_+ and m_- into the Landau-Lifshitz equation,

$$m_+=\sum_{\mathbf{k}} a_{\mathbf{k}} e^{i\mathbf{k}\cdot\mathbf{r}}, \quad m_-=\sum_{\mathbf{k}} a^*_{-\mathbf{k}} e^{i\mathbf{k}\cdot\mathbf{r}} . \tag{2}$$

This yields a set of equations of motion for the spin-wave coefficients, $a_{\mathbf{k}}$,

$$\frac{da_{\mathbf{k}}}{dt}=L_{\mathbf{k}}\begin{bmatrix} a_{\mathbf{k}} \\ a^*_{-\mathbf{k}}\end{bmatrix}+U_{\mathbf{k}}(a_{\mathbf{k}'}) ,$$

where $L_{\mathbf{k}}$ is a linear operator which acts only on the subset $a_{\mathbf{k}}$ and $a^*_{-\mathbf{k}}$ and $U_{\mathbf{k}}$ is the nonlinear term which, in general couples all the modes (coefficients), $a_{\mathbf{k}'}$.

At the third step we make a transformation to new mode variables $(b_{\mathbf{k}})$ in which $L_{\mathbf{k}}$ is diagonal with eigenvalues $\pm i\omega_{\mathbf{k}}$ which are the spin-wave frequencies, each associated with a spin-wave with wave vector $\mathbf{k}$. This gives the equations of motion

$$\frac{db_{\mathbf{k}}}{dt}=i\omega_{\mathbf{k}}b_{\mathbf{k}}+U'_{\mathbf{k}}(b_{\mathbf{k}}) , \tag{3}$$

where $U'=SU$ with S being the transformation from $a_{\mathbf{k}}$ to $b_{\mathbf{k}}$ $(b_{\mathbf{k}}=Sa_{\mathbf{k}})$.

The fourth step is to make a slow-time transformation[8] which is equivalent to using the method of averaging[27] on Eq. (3). We let $b_{\mathbf{k}}=c_{\mathbf{k}}(t)e^{i\omega_{\mathbf{k}}t}$. This eliminates the linear term and averages over the high frequencies $(\omega_{\mathbf{k}})$ which are in the GHz range to give equations of motion for low-frequency phenomena $(c_{\mathbf{k}})$ in the MHz or less range which are observed in the experiment. This gives the equations of motion

$$\frac{dc_{\mathbf{k}}}{dt}=U''_{\mathbf{k}}(c_{\mathbf{k}}) , \tag{4}$$

where $U''(c_{\mathbf{k}})$ is the averaged nonlinear term. The only terms which can survive are those for which $\omega_{\mathbf{k}}\sim\omega/2$ (first-order Suhl intability, our case) or $\omega_{\mathbf{k}}\sim\omega$ (second-order Suhl instability), where ω is the driving frequency. These are the equations to be solved, subject to a choice of which of the infinite number of modes $(c_{\mathbf{k}})$ will be included.

A final step in our case is to limit the number of modes to three, $c_{\mathbf{k}}$, $c^*_{-\mathbf{k}}$, and $c_{\mathbf{O}}$. As we have described above, this is a nonresonant experiment, so we do not include a resonater mode in our analysis. The mode $c_{\mathbf{O}}$ is the uniform mode and is the only mode present at low rf powers. It represents the uniform precession of the magnetization about the applied static field. The other two modes can be arbitrarily chosen, but in our case we chose $\mathbf{k}$ to be such that these modes represented some of the first modes excited at the Suhl instability.[3,27] In addition we used the typical approximation that, because of the symmetry of the equations of motion[13,14] $c_{-\mathbf{k}}=c_{\mathbf{k}}$. Note that this is not the same as simply setting $c_{-\mathbf{k}}=0$; extra terms and factors are still retained.

Damping can be included by simply adding a term like $-\eta_{\mathbf{k}}c_{\mathbf{k}}$ where $\eta_{\mathbf{k}}$ is determined from the damping coefficient in the Landau-Lifshtz equation.[3,27] In addition, one must include detuning terms,[3,13,14] $\Delta_{\mathbf{k}}$ $(\mathbf{k}\neq\mathbf{0})$ which allow for the fact that $\omega_{\mathbf{k}}$ is not exactly equal to $\omega/2$. The final equations have the form

$$\frac{dc_0}{dt}=ih\gamma-\eta_0c_0+u_0(1)c_kc_k^*c_0+u_0(2)c_0^2c_0+u_0(3)c_kc_k^*+u_0(4)c_k^2+u_0(5)c_0^*c_0 , \tag{5}$$

$$\frac{dc_k}{dt}=i\Delta_kc_k-\eta_kc_k+u_k(1)c_kc_0^*c_0+u_k(2)c_k^2c_k^*+u_k(3)c_0c_k^*+u_k(5)c_0^*c_k+u_k(6)c_0c_k , \tag{6}$$

where $u_0(i)$ and $u_k(i)$ are the coefficients for the nonlinear terms for the uniform mode (c_0) and the spin-wave mode (c_k), respectively. These coefficients contain terms from the effective field (applied, dipole, and exchange fields) resulting from the above analysis.

We solved these equations numerically using a 4–5 step Runge-Kutta algorithm with variable step size and continuous error checking at each step. The salient parameters were taken to be static field, $H_0=893.5$ G; $\gamma=1.758\times10^7$; saturation magnetization, $M_s=141.65$ G; damping $\eta_k=2.217\times10^6$ and $\eta_0=4.468\times10^6$; $k=5.25\times10^4$ cm^{-1}; $\theta_k=14.9°$; $\phi_k=0°$; and exchange, $D/M_s=2.262\times10^{-10}$ (see Refs. 3 and 27 for more details on these parameters). The parameter ranges in rf power and driving (resonant) frequency were adjusted to cover the same regimes as the experiment. The following results for $\omega=\omega_0=1.5708\times10^{10}$ Hz (=2.5 GHz driving frequency), $\omega_k=7.795\times10^9$ Hz ($=\omega/2$, the first-order Suhl instability), and rf field going from 10^{-4} to 10^{-1} G are typical for all solutions we found.

The overall behavior can be easily understood by looking at a bifurcation plot [Fig. 15(a)] in which the long-time behavior of the real part of $c_{\mathbf{k}}$ is plotted as a function of driving field, h. A similar plot results from using the imaginary part of $c_{\mathbf{k}}$. To make this plot we set the h value and chose the initial conditions at random. We then allowed the system to evolve for a time step of a few ms and plotted the next several hundred points separated by a time step of 100 ns. The value of h was then increased slightly, the initial conditions of the system were reset to random values, and the same plotting was done at the new h value. This was done for h values from ~1.8 to 8.0 mG.

This generated a plot in which it is easy to discern fixed-point behavior from periodic or chaotic behavior. The fixed points (seen at lower h values) represent $c_{\mathbf{k}}$=const. In certain cases, if the frequency of any periodic behavior can be found, the time steps can be set to strobe this trajectory and make it stand out as though it were a fixed point, too. Fourier transforms of non-fixed-point trajectories (above about 3.673 mG) showed no periodic behavior. Hence, on this plot 3.673 mG demarcates the boundary in the h parameter between fixed-point and chaotic behavior.

No periodic behavior implies that auto-oscillations appear to be absent from the three-mode model in the parameter regime we have explored. This is in agreement with the work of Bryant *et al.*[8] in which it was found that in off-resonance situations, for the first-order Suhl instability, auto-oscillations are missing from a three-mode model. In Bryant's case more modes must be added to the system to enable this behavior. It appears that this is so in our on-resonance situation, too.

We also did a linear stability study of the fixed-point solutions below the threshold for chaos. This is an analysis of whether the solutions are stable to small perturbations. The result of this is shown in Fig. 15(b). Stable fixed-point branches are shown to Re($c_{\mathbf{k}}$) in black and unstable parts of the branches are shown in gray shading.

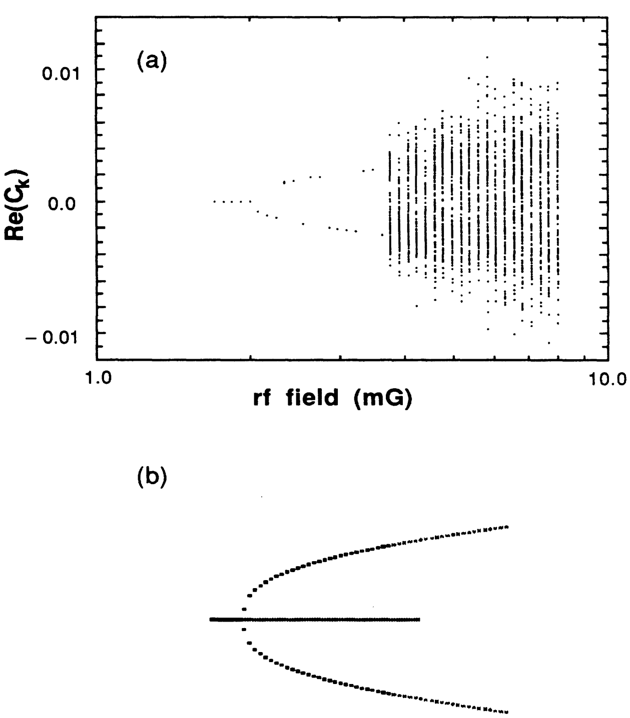

FIG. 15. (a) Bifurcation plot from a three-mode spin-wave model showing the Suhl instability at a dc field of 2.044 mG and the onset of chaos at 3.673 mG. (b) Stability analysis plot from the three-mode spin-wave model, showing stable fixed points (black) and unstable fixed points (gray).

Figure 15 then shows clearly the regimes of rf driving field where the spin-wave-mode amplitudes are constant or are chaotic. The Suhl instability near 2.044 mG is clearly visible (below this there are no spin waves, $c_{\mathbf{k}}=0$). At 2.044 mG there is a pitchfork bifurcation[8] and two, nonzero fixed points emerge. In this regime the spin waves have constant amplitude. This presumably happens in the experiment and is evidenced in the plots of reflectivity versus h (Fig. 12), but the constant behavior of the spin waves is not detectable by the digitization circuitry since we rely on time-dependent coupling to the uniform mode for the detection of the signals.

Above about 3.673 mG the system breaks into chaotic behavior. Just before this point we see very short ($\sim$ μs) chaotic transients over a very small range of rf field (~0.2 mG). Above the threshold for chaos, allowing the system to run for very long times (tens of ms) shows the same chaotic behavior as for short times. This would not be expected if there were transients present above 3.673 mG. While a three-mode is sufficient to produce chaotic transients it is not good enough to reproduce the long-lived transients that we see in the experiment.

Figure 16 shows a typical plot of the system behavior in the chaotic regime at a rf power of 4.0 mG. Three components [Re(c_0), Im(c_0), and Re(c_k)] of the four-component system are plotted. In the low power chaotic regimes, the system resembles the Lorenz attractor,[17] where the two fixed points have become hyperbolic fixed points. In the Lorenz attractor the two fixed points go unstable by a subcritical bifurcation.[17] From the stability

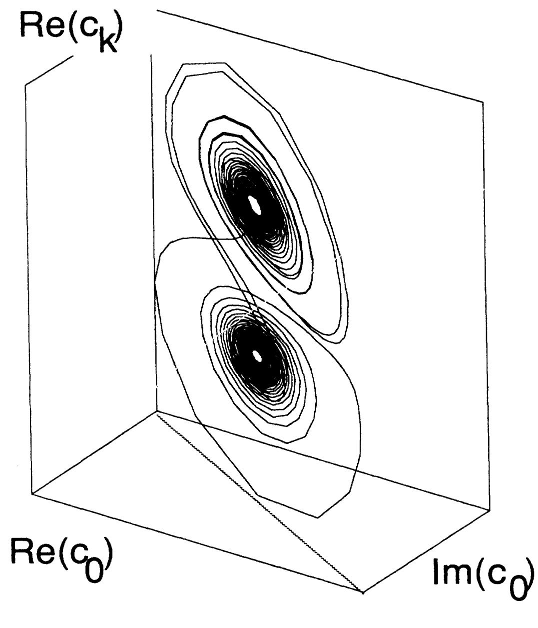

FIG. 16. Three-dimensional plot of a chaotic attractor for the three-mode spin-wave model. One component, the imaginary part of c_k, has been left for clarity.

analysis we can only say that if subcritical bifurcation occurs here, then the range over which the stable fixed-point branches and the strange attractor coexist is less than 1.0 mG. This is about 6×10^{-3} fractional part of the spin-wave fixed-point branch compared to about 3×10^{-2} fractional part of the two steady-state branch for the Lorenz attractor.

In the Lorenz attractor metastable chaos is detectable over about half of the two-steady-state branch. In our three-mode model it is detectable only over about 14% of the spin-wave steady-state range and the transients appear to be very short over most of this range. We have not made an examination of the scaling behavior of the transients, as we did for the experimental data.

It must be remembered that the system in Eq. (5) and (6) is a four-dimensional system, so that care must be taken in comparing details of the behavior to the three-dimensional Lorenz system.

While the three-mode model reflects a few aspects of the behavior of our experimental system, there are many phenomena that it does not model. This suggests that the complex behavior in the experiment results from the interaction of more than three spin-wave modes. This is also suggested by our analysis of the fractal dimension of the chaotic attractor and transients in the data. The fractal dimension saturates at an embedding dimension of 8, implying that the smallest dynamical model of the spin-wave system must have at least eight components. Work by others[8,13,14] in the nonresonant parameter regime also suggests that more than three modes are necessary.

ACKNOWLEDGMENTS

We would like to acknowledge useful conversations with E. Ott. We also acknowledge the help and encouragement of A. C. Ehrlich, A. W. Saenz, and C. D. Jeffries. One of us (T.L.C.) was supported by the Office of Naval Technology–American Society for Engineering Education.

[1]B. Lax and K. J. Button, *Microwave Ferrites and Ferrimagnetics* (McGraw-Hill, New York, 1961).
[2]W. Damon, in *Magnetism*, edited by G. T. Rado and H. Suhl (Academic, New York, 1963).
[3]H. Suhl, J. Phys. Chem. Solids **1**, 209 (1957).
[4]G. Gibson and C. Jeffries, Phys. Rev. A **29**, 811 (1984).
[5]T. L. Carroll, L. M. Pecora, and F. J. Rachford, Phys. Rev. Lett. **59**, 2891 (1987).
[6]T. L. Carroll, F. J. Rachford, and L. M. Pecora, Phys. Rev. B **38**, 2938 (1988).
[7]T. L. Carroll, L. M. Pecora, and F. J. Rachford, J. Appl. Phys. (to be published).
[8]P. Bryant, C. Jeffries, and K. Nakamura, Phys. Rev. A **38**, 4223 (1988).
[9]S. M. Rezende, O. F. de Alcantra Bonfim, and F. M. de Aguiar, Phys. Rev. B **33**, 5153 (1986).
[10]H. Yamazaki and M. Warden, J. Phys. Soc. Jpn. **55**, 4477 (1986).
[11]K. Nakamura, S. Ohta, and K. Kawasaki, J. Phys. C **15**, L143 (1982).
[12]S. Ohta and K. Nakamura, J. Phys. C **16**, L605 (1983).
[13]X. Y. Zhang and H. Suhl, Phys. Rev. A **32**, 2530 (1985).
[14]H. Suhl and X. Y. Zhang, Phys. Rev. Lett. **57**, 1480 (1986).
[15]C. D. Jeffries, Phys. Scr. **T9**, 11 (1985).
[16]A. Zettl, in *Methods and Applications of Nonlinear Dynamics*, edited by A. W. Saenz (World Scientific, Singapore, 1988), p. 203.
[17]Pierre Berge, Yves Pomeau, and Christian Vidal, *Order Within Chaos* (Wiley, New York, 1984).
[18]D. Ruelle and F. Takens, Commun. Math. Phys. **20**, 167 (1971).
[19]J. D. Farmer, E. Ott, and J. A. Yorke, Physica (Amsterdam) D **7**, 153 (1983).
[20]Y. Termonia and Z. Alexandrowicz, Phys. Rev. Lett. **51**, 1265 (1983).
[21]M. Gorman, P. J. Widmann, and K. A. Robbins, Phys. Rev. Lett. **52**, 2241 (1984).
[22]C. Grebogi, E. Ott, and J. A. Yorke, Ergod. Th. Dynam. Sys. **5**, 341 (1985).
[23]C. Grebogi, E. Ott, and J. A. Yorke, Phys. Rev. Lett. **57**, 1284 (1986).
[24]C. Grebogi, E. Ott, F. Romeiras, and J. A. Yorke, Phys. Rev. A **36**, 5365 (1987).
[25]Similar phenomena have been observed by H. Benner, F. Rodelsperger, H. Seitz, and G. Wiese, in Proceedings of the International Conference on Magnetism, Paris, 1988 (Les Editions de Physique, Paris, in press).
[26]L. D. Landau and E. M. Lifshitz, Phys. Z. Sowjetunion **8**, 153 (1935), reproduced in *Collected Papers of L. D. Landau,*, edited by D. ter Haar (Pergamon, New York, 1965).
[27]L. M. Pecora, Phys. Rev. B **37**, 5473 (1988).